Journal of the European Ceramic Society 16 (1996) 945–952
© 1996 Elsevier Science Limited
Printed in Great Britain. All rights reserved
S0955-2219(96)00015-5
0955-2219/96/$15.00

Low-temperature Sintering and Microstructural Development of Nanocrystalline Y-TZP Powders

P. Durán, M. Villegas, F. Capel, P. Recio & C. Moure

Instituto de Cerármica y Vidrio (CSIC), Electroceramics Department, 28500 Arganda del Rey, Madrid, Spain

(Received 29 September 1995; revised version received 12 December 1995; accepted 5 January 1996)

Abstract

Powders of yttria-doped tetragonal zirconia (3 mol%) with a narrow pore size distribution and ultrafine particle size (~9 nm) have been prepared by the mixed organic + inorganic precursors coprecipitation method. The compaction behaviour of almost agglomerate-free calcined powders was studied, and their sintering behaviour using both isothermal and non-isothermal techniques was evaluated. Fully dense nanoscale ceramics with an average grain size below 95 nm were obtained after sintering at 1200°C for 20 min or at 1150°C for 4 h. Several stages were identified in the whole densification process: it was found that a particle rearrangement process assisted by sintering pressure is the densification mechanism in the earlier sintering step (up to 800°C), and grain boundary diffusion was the dominant mechanism for densification up to 1180°C. Activation energy values of 130 ± 20 and 300 ± 40 kJ mol^{-1}, respectively, were calculated for these densification mechanisms. The almost complete absence of agglomerates in the calcined powders and the homogeneous pore structure of the green compacts are the two main factors leading to low-temperature fully densified Y-TZP bodies. © 1996 Elsevier Science Limited.

1 Introduction

The use of advanced ceramics for structural applications or as electronic components will become more generalized when all the problems associated with their development, such as poor sinterability without aids, normally low densities, internal flaws and degraded mechanical properties as a consequence of the internal holes, can be solved. Much effort has been made over the years to circumvent the above-mentioned obstacles, and, today, the control of both powder synthesis and subsequent sintering to achieve high density and ultrafine grained microstructure in the sintered bodies is still one of the major challenges in the processing of ceramic materials. To the latter end, the use of nanocrystalline ceramic powders could be the key for achieving much lower sintering temperatures, better microstructures, improved mechanical and electrical properties and, as a consequence, higher reliability.

Different methods such as sol–gel,[1,2] hydrothermal synthesis,[3] spray pyrolysis[4] or, more recently, electrochemical synthesis[5] are used for making nanocrystalline ceramic powders. Although the solution methods present some disadvantages related mainly to the drying and purity of the powders, their low cost and relatively good reproducibility make them more attractive from the viewpoint of a possible industrial application. Thus, in spite of some difficulties, the aqueous coprecipitation methods are the most widely used to prepare nanoscale ceramic powders.

In the case of fully stabilized tetragonal Y_2O_3–ZrO_2 ceramics (Y-TZP), it is well known that the room-temperature phase stability, strength and toughness depend strongly on a critical grain size (<0.8 μm), and that the requirement is so strict when Y-TZP ceramics are exposed to humid atmospheres that the above critical grain size has to be reduced to ~0·25 μm.[6,7] Because of this, the production of nanostructured ceramics is very interesting not only for the above advantages but also because, when coupled with attention to forming methods, it is favourable for achieving superplastic behaviour at relatively high temperatures.[8,9]

The present work was undertaken to study the sintering behaviour and the microstructural development of a nanocrystalline Y-TZP (3 mol% Y_2O_3) powder prepared by a mixed organic–inorganic precursors coprecipitation method.

2 Experimental Procedure

2.1 Powder preparation

The preparation of amorphous Y-TZP (3 mol% Y_2O_3) powders was carried out by dissolving, in the adequate proportions, yttrium nitrate [$Y(NO_3)O_3 \cdot 5H_2O$] and zirconium tetrabutoxide [$Zr(C_4H_9O)_4 \cdot C_4H_9OH$] in slightly acidulated isopropyl alcohol. Complete coprecipitation of the Y^{3+} and Zr^{4+} cations was achieved by mixing with an excess of 12 N aqueous ammonia solution using a procedure similar to that previously reported to obtain Er-TZP amorphous powders;[10] the details of the basic procedure were described in the previous report and will not be repeated here. However, we would like to emphasize some points: (1) the order of addition of the reactants was that of dropping the above acidic cation solution to the stirred, aqueous ammonia solution, resulting in a simultaneous and homogeneous coprecipitation under the precipitation conditions (pH > 9); (2) the sequence of the washing process was water → water + isopropyl alcohol mixture → anhydrous isopropyl alcohol for two or three times; and (3) the washed powders were calcined at 500°C for 1 h. These and all the other powder preparation steps mentioned elsewhere[10] have to be rigorously controlled in order to achieve unagglomerated or weakly agglomerated nano-sized Y-TZP powders.

2.2 Powder characterization

Crystallite sizes of calcined powders were determined by means of the X-ray line broadening (XRLB) method[11] using an X-ray diffractometer (Siemens D5000), Cu K_α radiation and a scan rate of 0·5° min^{-1}. The crystallite size, D, was calculated from the Scherrer equation:

$$D = 0.9\lambda/(\beta \cos\theta)$$

where λ is the wavelength of the X-rays, θ is the diffraction angle and β is the calibrated width of the diffraction peak at half-maximum at the selected 2θ. Particle size and shape were also examined by transmission electron microscopy (TEM; ME-300, Philips) and scanning electron microscopy (SEM; DSM-950, Carl Zeiss). Specific surface area was measured by the BET (Accusorb 210E, Micromeritics) method, and the amorphous powders were also characterized by means of dynamic thermal analysis/thermogravimetric analysis (DTA/TG; Netzsch STA-409).

2.3 Powder compaction and sintering

After calcining, the powders were isopressed at different compaction pressures up to 350 MPa, and the compaction behaviour was studied by measuring the changes in density with increased isostatic pressure. The pore size distribution in both the green and the sintered compacts was calculated by mercury porosimetry (Autopore II 9215). Sintering kinetics were studied by non-isothermal experiments using constant-rate heating (CRH) dilatometry (Netzsch DIL 402E/7) at a heating rate of 5°C min^{-1} from 200 to 1400°C. Isothermal sintering was performed at different temperatures at a heating rate of 5°C min^{-1}. After sintering, the samples were quickly cooled to room temperature. The density of the sintered samples was measured by Archimedes' method with water, and grain size was measured by X-ray line broadening and/or by SEM using the interception method.[12]

3 Experimental Results

3.1 Powder characteristics

As shown in Fig. 1, the thermogravimetry curve shows that only about 12% total weight loss occurs on heating, which is much smaller than that corresponding to a well formed Y–Zr hydroxide. This result and the exothermic peak centred at ~140°C in the DTA curve indicate that the majority of the adsorbed water has been eliminated during the drying at 300°C to remove residual anhydrous isopropyl alcohol.[10] The exothermic peak at 440°C in the DTA curve indicates that the crystallization of tetragonal zirconia starts at about 400°C and ends at about 500°C, in fairly good agreement with previous results.[13] For this reason, as mentioned above, the coprecipitated powders were calcined at a temperature at which the complex Y–Zr hydroxide would completely transform to tetragonal zirconia and for a short time, to avoid excessive crystallite growth.

The as-prepared powders were amorphous as determined by X-ray diffraction, and the powders calcined at 500°C for 1 h were not well crystallized tetragonal yttria-doped zirconia solid solution. The surface areas of the isopropyl alcohol washed coprecipitated yttria–zirconia powders were in the range 200–250 $m^2\ g^{-1}$. The calcined powders had surface areas S_{BET} in the range 80–90 $m^2\ g^{-1}$ and a crystallite size of ~9 nm as calculated by XRLB analysis. The crystallite diameter calculated from S_{BET}, using the equation $D = 6/(\rho_t \cdot S_{BET})$ in which ρ_t is the theoretical density, was in the range 10–12 nm. A TEM micrograph of the calcined powders (see Fig. 2) shows a weakly agglomerated powder in which an average crystallite size of ~10 nm could be measured, in close agreement with the above measurements. Some agglomerate-like chains (three to five

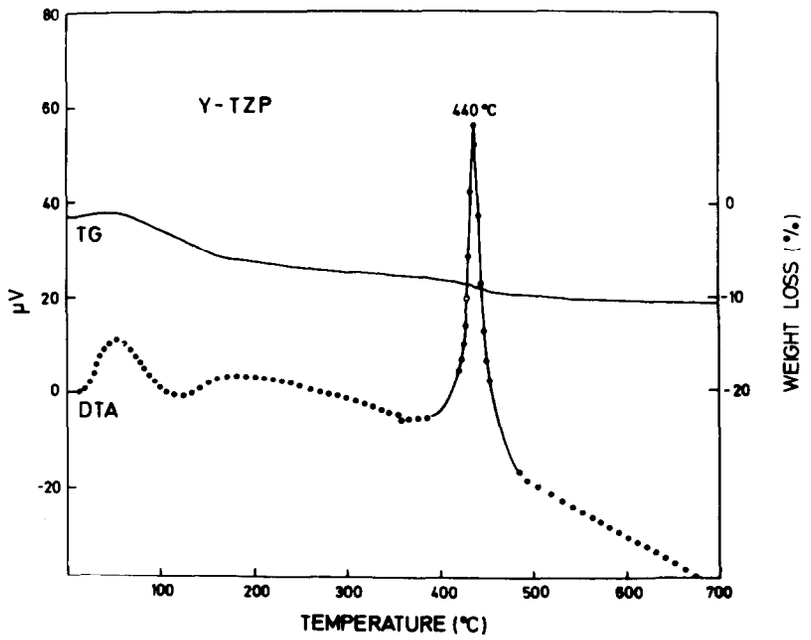

Fig. 1. DTA/TG curves for Y-TZP coprecipitated powders.

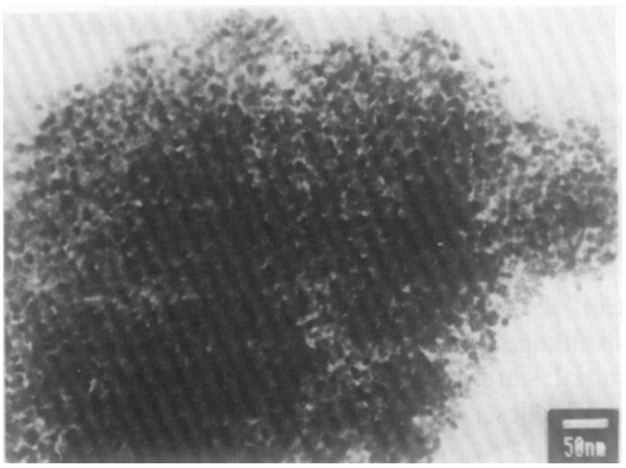

Fig. 2. Transmission electron micrograph of Y-TZP calcined powders.

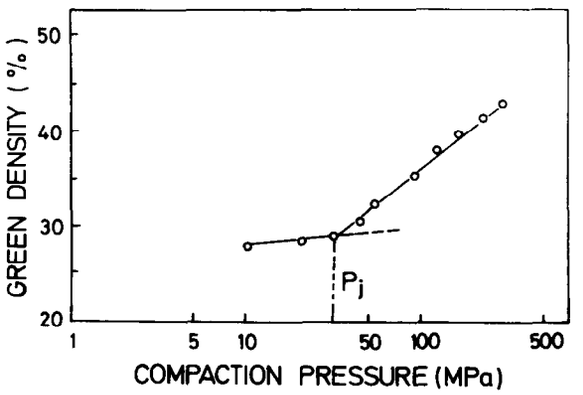

Fig. 3. Compaction behaviour of the nano-sized Y-TZP calcined powders.

primary crystallites apparently welded by necks or overlapped) can be observed. These characteristics reveal that, after calcining, the powder is in a loose state with high internal porosity which facilitates the destruction of the smaller agglomerates during milling.

3.2 Compaction behaviour

The compaction response of the calcined powders was studied by plotting the relative density of the green compacts vs. the logarithm of the applied pressure;[14] as shown in Fig. 3, a curve with two linear regions was obtained. In the first one, for compaction pressures lower than 40 MPa, variation in densification was barely achieved and this is consistent with a rearrangement of the soft agglomerates during pressing. The low break point (P_j < 40 MPa) in the curve, which is related to the agglomerate strength,[15] gives an idea of the weakness of the agglomerates which easily deform as a result of their lower strength.

In the second linear part of the curve (Fig. 3), the relative density increases with the compaction pressure, the agglomerates are deformed or fractured and the interagglomerate porosity, if any, is eliminated. No advantage in the sintering process is gained by exceeding 250 MPa (~43% dense), and at the end a coherent compact structure with a narrow pore size distribution is obtained (see Fig. 4). This result is consistent with the above assumption of a high internal powder porosity leading to green compacts with inter- and intraagglomerate pores with the same dimensions.

Given that the average pore diameter (~6 nm) and the average crystallite size (9–10 nm) are quite similar, the simpler cubic rearrangement for the crystallites in the green compacts could be assumed. From the average crystallite size, the calculated pore diameter (assuming spherical crystallites) is approximately 4 nm for such a cubic

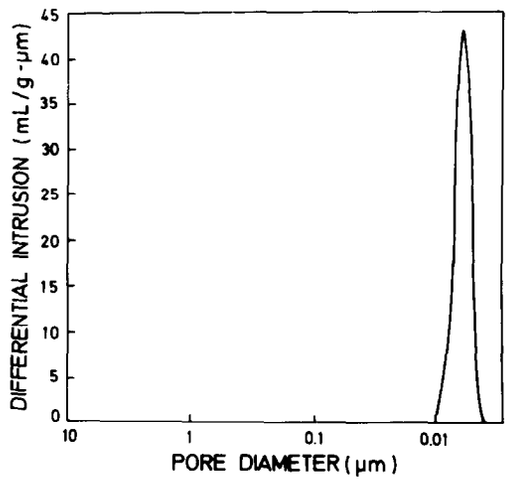

Fig. 4. Pore size distribution in the Y-TZP green compacts.

arrangement. This value is in reasonable agreement with the observed mode size of 6 nm in Fig. 4. This result and the low green density of the compacts (~43% theoretical density), which is considerably below the value for a close-packed structure, lead us to assume the presence of many small packing defects — undetected by Hg porosimetry — between the crystallite arrangements leading to packing inhomogeneities (dislocations, grain boundaries, some agglomerates that are not destroyed, etc.) in the green compacts. Since (as mentioned above) the crystallite size calculated from S_{BET} and by XRLB is almost the same and the pore size distribution in green compacts shows a single mode size of 6 nm, it can be concluded that the calcined powder is agglomerate-free and the porosity in our compacts is mainly intercrystallite.

3.3 Constant-rate heating densification experiments

Non-isothermal densification experiments in air showed that the compacts start to shrink at ~500°C, the temperature for 4% shrinkage being ~800°C, and that the shrinkage process (total shrinkage ~26%) is complete at approximately 1250°C. In terms of the relative density, calculated from the initial green density and the shrinkage data, Fig. 5(A) shows that, up to ~1000°C (12% shrinkage), a densification of only 15% (from 43 to 58% theoretical density) takes place. In the short temperature interval of 250°C, between 1000 and 1250°C, a strong shrinkage and a rapid densification (97% theoretical density) were achieved. At ~1275°C the density was as high as 99·9%. According to the experimental curve obtained for densification rate during sintering, shown in Fig. 5(B), the maximum densification rate is found at a temperature as low as 1180°C, proving the high sinterability of the prepared compacts. The presence of only one maximum in the densification rate curve confirms the single mode and narrow

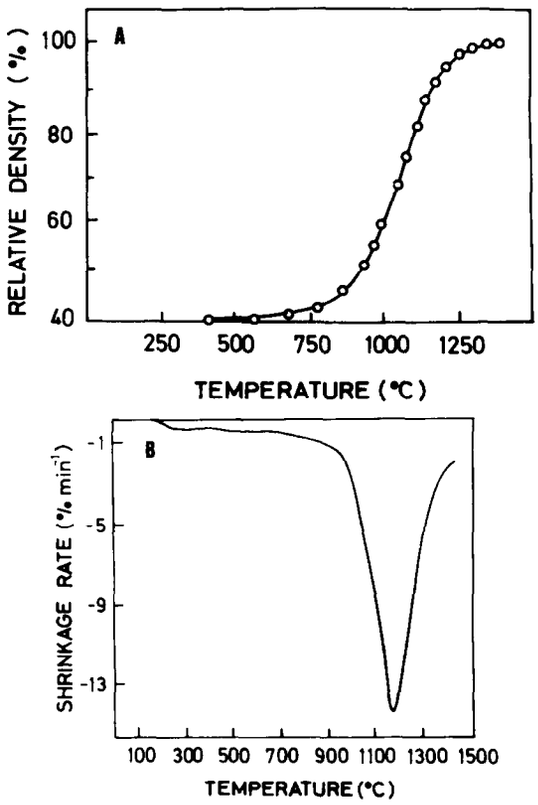

Fig. 5. Non-isothermal sintering behaviour of Y-TZP compacts: (A) densification vs. temperature; and (B) shrinkage rate curve.

pore size distribution in the compacted samples.

Sintering kinetics for Y-TZP powder compacts can be analysed on the basis of initial sintering shrinkage. According to Young and Cutler,[16] the initial sintering theory with constant-rate heating can be described by the expression:

$$\ln\left(\frac{\Delta l/l_o}{T}\right) = \frac{-nQ}{RT} + C$$

where $\Delta l/l_0$ is the fractional shrinkage of the compact at temperature T, Q is the activation energy, and C and n are constants related to the powder geometry and the sintering mechanism, respectively. RT has its usual meaning. Figure 6 shows a plot of the experimental data for $\ln(\Delta l/l_0)/T$ vs. $1/T$ and, as was expected for compacts which are relatively inhomogeneous in packing, the Arrhenius plot is not completely linear over the whole range of densification.

This result suggests that the densification process can be divided into several stages. In a first stage, up to ~800°C, if it is assumed that $n = 0{\cdot}3$ in the above equation, which is the value for a grain boundary diffusion mechanism, an activation energy of 130 ± 20 kJ mol^{-1} was calculated: this is too low to be associated with such a diffusion mechanism at the early stage of densification. According to the results of Fig. 5(B), the low shrinkage rate at this densification stage seems to be better correlated to a rearrangement process in

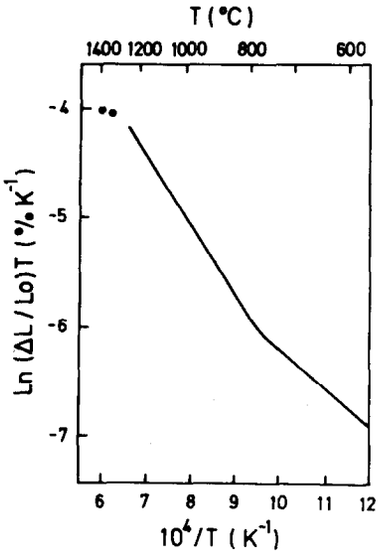

Fig. 6. Arrhenius plot of logarithm of shrinkage vs. the reciprocal of temperature.

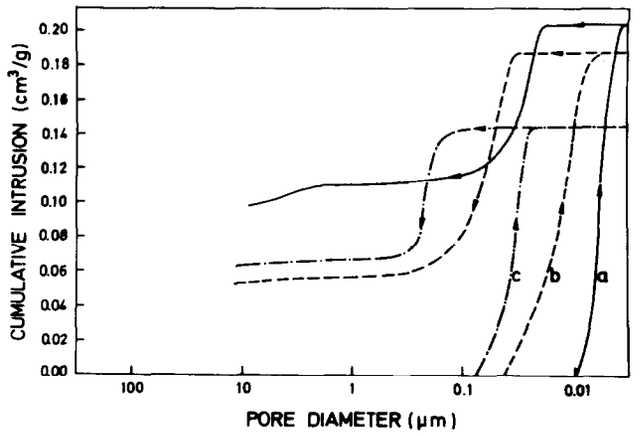

Fig. 7. Hysteresis curves of mercury porosimetry for (a) as-pressed Y-TZP compacts, (b) sintered at 620°C, and (c) sintered at 980°C.

which the porosity of the intercrystallite arrays is transported to the surface of the crystallite arrays with a subsequent densification of the crystallite arrays. This results in a slight densification of the compact in which a change of both the microstructure and the morphology of the pores has been produced.

To confirm the above assumption, a study of the intruded–extruded mercury was made by mercury porosimetry[17] on as-pressed compacts and those sintered at 620 and 980°C. As shown in Fig. 7, a different intruded/extruded mercury ratio was found and this was lower in the case of the compacts sintered at 980°C (average pore diameter = 30 nm) than in those sintered at 620°C (average pore diameter = 15 nm) or in the as-pressed compacts. This means that some entrapment of mercury in pores took place in the latter case mainly due to the small entrance openings, and the fact that a larger volume of mercury was extruded during the depressurizing process indicates that both the entrance size and the interior are quite similar in the former cases. This result and the microstructure in Fig. 8 lead us to assume that an evolution of the pore shape, from spheroidal to interconnected columnar or cylindrical, occurs with temperature. In conclusion a new pore configuration at the end of the early sintering stage, as consequence of the particle rearrangement process, seems to exist. Such a rearrangement process assisted by the sintering pressure as the driving force[18,19] can be considered as the main mechanism responsible for the early densification stage.

A second densification stage seems to be present between ~800 and 1180°C in which an extremely high shrinkage rate takes place (see Fig. 5(B)). From $n = 0{\cdot}25$ reported elsewhere for this temperature range[20] and the slope calculated in Fig. 6, a value of $Q = 300 \pm 40$ kJ mol^{-1} for the activation energy was calculated. This is somewhat higher than the values reported by Theunissen *et al.*[21] (275 kJ mol^{-1}) for a commercial Y-TZP powder and by Durán *et al.*[10] (270 ± 40 kJ mol^{-1}) for a nanoscale Er-TZP powder. Although the activation energy reported here is somewhat lower than that corresponding to a single grain boundary diffusion mechanism[22] (385 kJ mol^{-1}), such a diffusion mechanism is more effective for densification than volume diffusion and, therefore, grain boundary diffusion was assumed to be the main densification mechanism present between 800 and 1180°C. Over this temperature interval a rapid densification takes place, the relative density increasing from about 48 to 97% theoretical density. It is believed that, favoured by the new pore configuration and the sintering pressure, the pores are rapidly eliminated along the grain boundaries, at least in the beginning of this second densification stage. The little grain growth observed at this point indicates that the mobility of the pores was much higher than that of the grain boundaries. Thus the pores, being much smaller than the grain size, and their mobility are believed to have a pinning effect for the grain boundaries and, hence, for grain growth. With increasing relative density and after a certain pore coalescence, the effect of sintering pressure becomes incrementally smaller.[19] Theunissen *et al.*[21] reported a sintering pressure of 70 MPa at 900°C and suggested that at this stage, densification can still be considerable. At 1180°C the relative density was higher than 95% and the average pore diameter was 70 nm: this indicates that the pore surface curvature is small and, therefore, the sintering pressure and its effect on densification will also be very small.[18]

Above 1180°C, a third densification stage could be present. Almost complete densification, about 99·9% theoretical density, is attained and normal

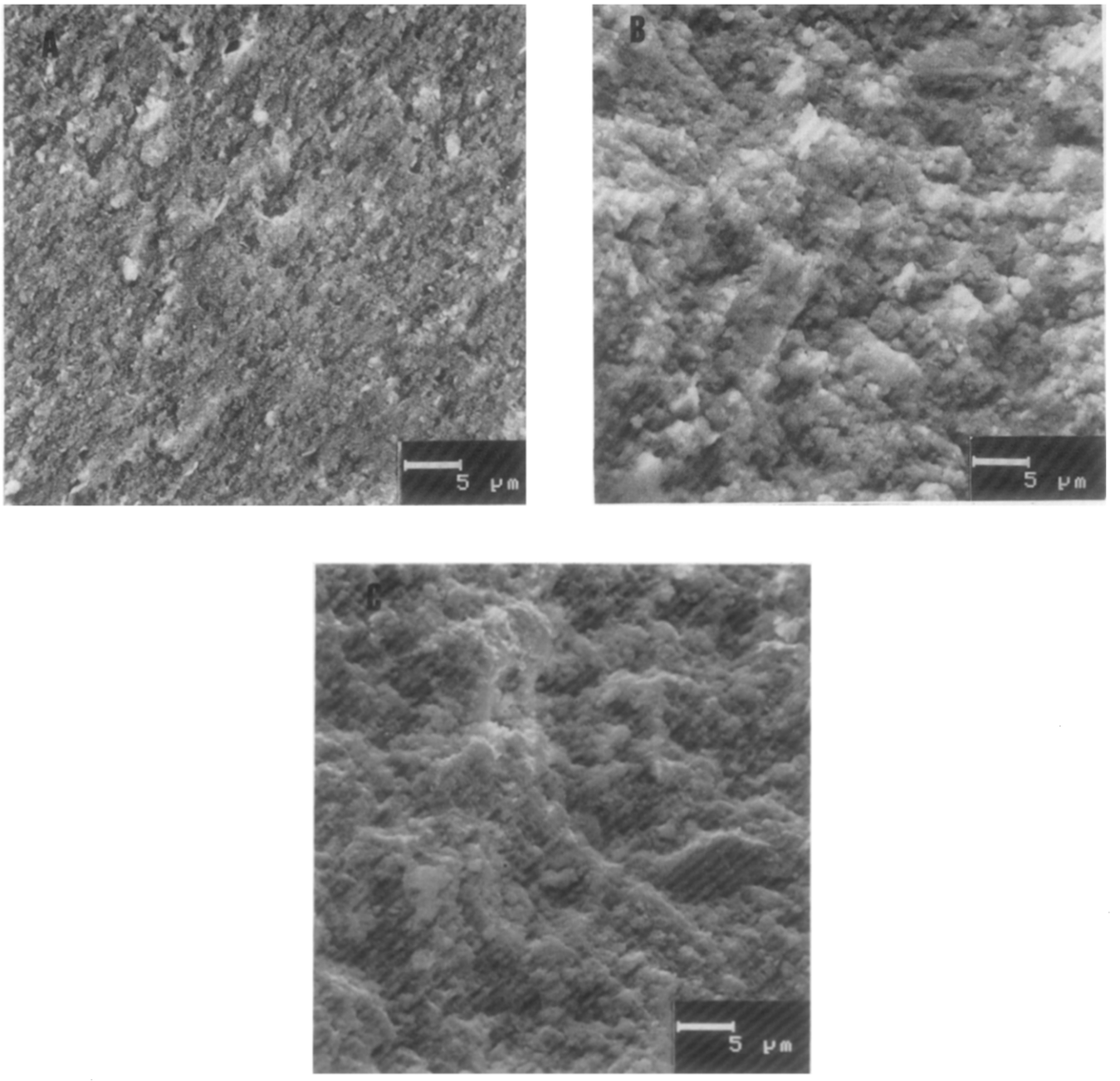

Fig. 8. Microstructure of fracture surfaces in Y-TZP compacts: (A) as-pressed, (B) sintered at 620°C, and (C) sintered at 980°C.

grain growth was observed. At this sintering stage volume diffusion was assumed as the main densification mechanism.

3.4 Isothermal densification

Isothermal sintering behaviour of the Y-TZP powder compacts was studied at temperatures for which the densification was nearly complete and the grain size in the nanometre range. Thus, one of these experiments was performed at the second densification stage (i.e. at 1150°C) and the other at 1200°C (i.e. at the third densification stage). Figure 9 shows the isothermal densification curves for samples sintered at the chosen temperatures. As can be observed, the time dependence of the density was very different at and above 1150°C. At this temperature the density increased continuously, whereas above it the Y-TZP ceramics were fully dense within the first 10–15 min. In the samples sintered at 1150°C, starting with a relative density of 55%, a relative density of 95% was obtained after only 50 min of heat treatment and fully dense bodies were achieved after 4 h. A grain size as low as 85 nm was measured at this point.

In the case of the samples sintered at 1200°C, fully dense Y-TZP ceramics were obtained for sintering times shorter than 20 min with a grain size still below 100 nm. The rapid initial densification confirms the statement that a particle rearrangement process assisted by sintering pressure[23] plays

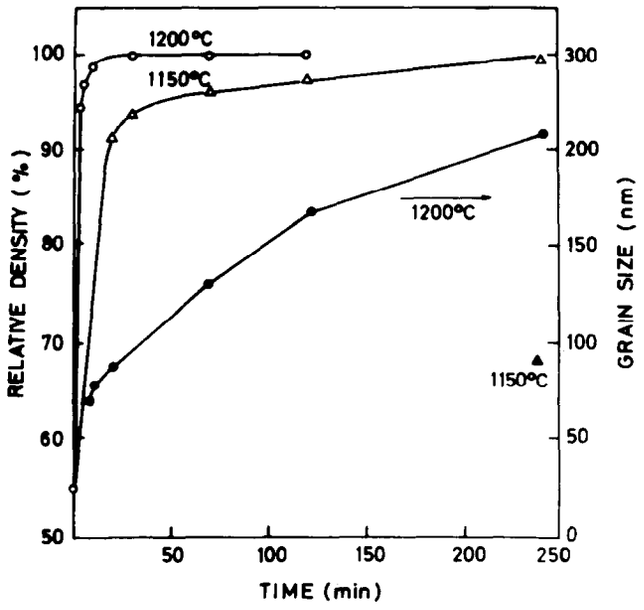

Fig. 9. Isothermal densification behaviour and grain size of Y-TZP compacts as functions of temperature and time.

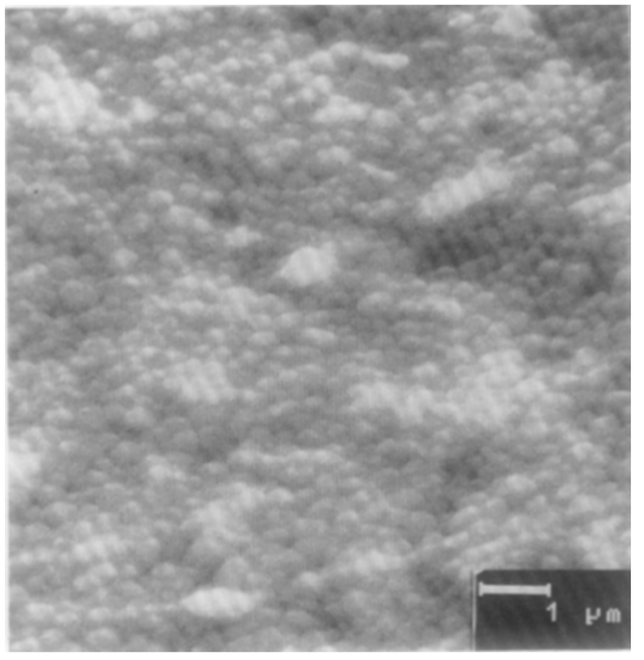

Fig. 10. Microstructure of fully dense Y-TZP compact sintered at 1200°C for 240 min.

an important role in rapid pore elimination at the early densification stage. For longer sintering times the relative density remains constant and relatively rapid grain growth takes place. A grain size of 210 nm was measured after 4 h of sintering (see Fig. 10), which indicates that at this temperature volume diffusion is probably the most important diffusion mechanism. The fact that Y-TZP fully dense ceramics have been obtained at low temperatures (1150–1200°C) with a grain size within the nanometre range (<100 nm) makes it an interesting material for superplastic forming applications. Nanostructured Y-TZP and YCe-TZP ceramics with relatively high densities (90–93% theoretical density) sintered at a temperature as low as 1100°C, using sinter forging as a pressure-assisted densification technique, have recently been reported.[24]

4 Conclusions

From the above experimental results, the following conclusions may be drawn.

(1) Highly sinterable Y-TZP calcined powders, having specific surface areas as high as 90 $m^2\ g^{-1}$ and an average crystallite size of 8–10 nm, can be prepared by the mixed organic and inorganic precursors coprecipitation method.

(2) Owing to the unusual characteristics of the Y-TZP calcined powders (very small and soft arrays of three to five particles) and the sharp pore size distribution in the green compacts, fully dense ceramics with a grain size in the nanometre range (<100 nm) were obtained at a sintering temperature as low as 1150°C for 4 h or at 1200°C for much shorter (~20 min) sintering times.

(3) From the constant-rate heating sintering experiments several (at least three well defined) densification steps could be established but it was very difficult to determine the start and the end of each of them. A first step comprising a particle rearrangement process assisted by sintering pressure seems to be present up to ~800°C. The low activation energy value calculated for this densification step (130 ± 40 kJ mol^{-1}) cannot be associated with any of the known diffusional mechanisms. A second densification step, in which rapid densification (≥ 95% dense) occurs with slow grain growth, takes place between 800 and 1180°C, and it was considered as the most important in the whole densification process. The activation energy value calculated for this second densification step (300 ± 40 kJ mol^{-1}) could be well correlated to grain boundary diffusion as the main densification mechanism. Finally, a third densification step is considered to exist above 1180°C in which almost fully dense Y-TZP ceramics were achieved. At this densification step a normal grain growth process occurred, and volume diffusion was assumed to be the dominant densification mechanism.

(4) From the isothermal sintering experiments at 1150 and 1200°C, it can be stated that the rapid initial densification indicates an important role of the particle rearrangement

in the early densification step, supporting the above contention. Such a particle rearrangement process led to a new pore configuration which favoured both pore elimination along the grain boundaries and rapid densification during the first minutes in the second sintering stage.

(5) The small crystallite size of the Y-TZP calcined powders, the small crystallite arrays in the compacts, and the low activation energy for densification leading to dense ceramics at low temperature, in spite of the low green compact density, reveal the usefulness of the mixed organic–inorganic precursors precipitation method for preparing highly sinterable Y-TZP powders.

Acknowledgement

This research was supported in part by the European Commission under contract JOUE-044C.

References

1. Mackenzie, J. D., Applications of sol–gel methods for glass and ceramics processing. In *Ultrastructure Processing of Ceramics, Glasses and Composites*, eds L. L. Hench & D. R. Ulrich. Wiley, New York, 1984, pp. 15–26.
2. Barringer, E. A. & Bowen, H. K., Formation, packing and sintering of nanodisperse TiO_2 powders. *J. Am. Ceram. Soc.*, **65** (1982) c-199–201.
3. Zhou, Y. C. & Rahaman, M. N., Hydrothermal synthesis and sintering of ultrafine CeO_2 powders. *J. Mater. Res.*, **8** (1993) 1680–6.
4. Dubois, B., Ruffier, R. & Odier, P., Preparation of fine spherical yttria stabilized zirconia by the spray pyrolysis method. *J. Am. Ceram. Soc.*, **72** (1989) 713–15.
5. Zhou, Y. C., Phillips, R. J. & Switzer, J. A., Electrochemical synthesis and sintering of nanocrystalline cerium oxide powders. *J. Am. Ceram. Soc.*, **78** (1995) 981–5.
6. Lange, F. F., Transformation-toughened ZrO_2: Correlations between grain size control and composition in the system ZrO_2–Y_2O_3. *J. Mat. Sci.*, **17** (1982) 240–2.
7. Winnubst, A. J. A. & Burggraaf, A. J., The aging behaviour of ultrafine-grained Y-TZP in hot water. In *Advances in Ceramics, Vol. 24A, Science and Technology of Zirconia III*, eds S. Somiya, N. Yamamoto & H. Yanagida. The American Ceramic Society, Inc., Columbus, OH, 1989, pp. 39–47.
8. Panda, P. C., Wang, J. & Raj. R., Sinter forging characteristics of fine-grained zirconia. *J. Am. Ceram. Soc.*, **71** (1988) c-507–9.
9. Boutz, M. M. R., Winnubst, A. J. A., Burggraaf, A. J., Nauer, M. & Carry, C., Low temperature superplastic flow of Y-TZP. *J. Eur. Ceram. Soc.*, **13** (1994) 103–11.
10. Durán, P., Recio, P., Jurado, J. R., Pascual, C. & Moure, C., Preparation, sintering and properties of translucent Er_2O_3 doped tetragonal zirconia. *J. Am. Ceram. Soc.*, **72** (1989) 2088–93.
11. Klug, K. P. & Alexander, L. E., *X-Ray Diffraction Procedures*. John Wiley and Sons, New York, 1974.
12. Fullman, R. L., Measurement of particle size in opaque bodies. *J. Metals, Trans. AIME*, **197** (1953) 447–52.
13. Navarro, L., Recio. P. & Durán, P., Preparation and properties evaluation of zirconia-based/Al_2O_3 composites as electrolytes for solid oxide fuel cells systems. *J. Mater. Sci.*, **30** (1995) 1931–8.
14. Niesz, D. E., Benet, R. B. & Snyder, H. J., Strength characterization of powder aggregates. *Am. Ceram. Soc. Bull.*, **51** (1972) 677–80.
15. Matsumoto, R. L. K., Analysis of powder compaction using compaction rate diagram. *J. Am. Ceramic. Soc.*, **73** (1990) 465–8.
16. Young, W. S. & Cutler, I. B., Initial sintering with constant rate of heating. *J. Am. Ceram. Soc.*, **53** (1970) 659–63.
17. Petzow, G. & Exner, H. E., Particle rearrangement in solid state sintering. *Z. Metalled*, **67** (1976) 611–8.
18. Raj, R., Analysis of the sintering pressure. *J. Am. Ceram. Soc.*, **70** (1987) c-210–11.
19. Venkatachari, K. R. & Raj, R., Shear deformation and densification of powder compacts. *J. Am. Ceram. Soc.*, **69** (1986) 499–506.
20. Olmo, L. D., Durán, P. & Moure, C., Sintering of a Yttria-stabilized zirconia. In *Materials Science Monographs, Vol. 14, Sintering Theory and Practice*, eds D. Kolar, S. Pejonik & M. M. Ristic. Elsevier, Amsterdam, The Netherlands, 1982, pp. 401–8.
21. Theunissen, G. S. A. M., Winnubst, A. J. A. & Burggraaf, A. J., Sintering kinetics and microstructure development of nanoscale Y-TZP ceramics. *J. Eur. Ceram. Soc.*, **11** (1993) 315–24.
22. Jorgensen, P. J., Diffusion-controlled sintering oxides. In *Sintering and Related Phenomena*, eds G. C. Kuzynski, N. A. Hooton & C. F. Gibbon. Gordon and Breach, New York, 1967, pp. 401–22.
23. GrootZevert, W. F. M ., Winnubst, A. J. A., Theunissen, G. S. A. M. & Burggraaf, A. J., Powder preparation and compaction behaviour of fine-grained Y-TZP. *J. Mater. Sci.*, **25** (1990) 3449–55.
24. Boutz, M. M. R., Winnubst, L., Burggraaf, A. J., Nauer, M. & Carry, C., Low temperature sinter forging of nanostructured Y-TZP and YCe-TZP. *J. Am. Ceram. Soc.*, **78** (1995) 121–8.